An exercise-induced metabolic shield in distant organs blocks cancer progression and metastatic dissemination

Running Title: Exercise-induced metabolic shield blocks cancer progression and metastasis

Conflict of Interest:

The authors declare no potential conflicts of interest.

Danna Sheinboim[1,*], Shivang Parikh[1,*], Paulee Manich[1,*], Irit Markus[2], Sapir Dahan[1], Roma Parikh[1], Elisa Stubbs[2], Gali Cohen[2,4], Valentina Zemser-Werner[5], Rachel E. Bell[1], Sara Arciniegas Ruiz[1], Ruth Percik[6,7], Ronen Brenner[8], Stav Leibou[1], Hananya Vaknine[9], Gali Arad[1], Yariv Gerber[2,4], Lital Keinan-Boker[10,11], Tal Shimony[11], Lior Bikovski[12,13], Nir Goldstein[2], Keren Constantini[2], Sapir Labes[14], Shimonov Mordechai[1,15], Hila Doron[16], Ariel Lonescu[17], Tamar Ziv[18], Eran Nizri[6,19], Guy Choshen[6,20], Hagit Eldar-Finkelman[1], Yuval Tabach[14], Aharon Helman[22], Shamgar Ben- Eliyahu[21,23], Neta Erez[16], Eran Perlson[17,23], Tamar Geiger[24], Danny Ben-Zvi[25], Mehdi Khaled[3‡], Yftach Gepner[2‡], and Carmit Levy[1‡]

[1] Department of Human Genetics and Biochemistry, Sackler Faculty of Medicine, Tel Aviv University, Tel Aviv 69978, Israel.

[2] Department of Epidemiology and Preventive Medicine, School of Public Health, Sackler Faculty of Medicine, and Sylvan Adams Sports Institute, Tel-Aviv University, Tel-Aviv 69978, Israel.

[3] INSERM 1186, Gustave Roussy, Université Paris-Saclay, Villejuif 94805, France.

[4] Stanley Steyer Institute for Cancer Epidemiology and Research, Tel Aviv University, Tel Aviv 69978, Israel.

[5] Institute of Pathology, Tel Aviv Sourasky Medical Center, Tel Aviv 6423906, Israel.

[6] Sackler School of Medicine, Tel Aviv University, Tel Aviv 69978, Israel.

[7] Institute of Endocrinology, Chaim Sheba Medical Center, Tel Hashomer 52621, Israel.

[8] Institute of Oncology, E. Wolfson Medical Center, Holon 58100, Israel.

[9] Institute of Pathology, E. Wolfson Medical Center, Holon 58100, Israel.

[10] School of Public Health, Faculty of Social Welfare and Health Sciences, University of Haifa, Haifa 3498838, Israel.

[11] Israel Center for Disease Control, Israel Ministry of Health, Ramat Gan 5262160, Israel.

[12] The Myers Neuro-Behavioral Core Facility, Tel Aviv University, Tel Aviv 69978, Israel.

[13] School of Behavioral Sciences, Netanya Academic College, Netanya 4223587, Israel.

[14] Department of Developmental Biology and Cancer Research, Institute of Medical Research-Israel-Canada, The Hebrew University of Jerusalem, Jerusalem 9112102, Israel.

[15] Department of Surgery, E. Wolfson Medical Center, Holon 58100, Israel.

[16] Department of Pathology, Sackler Faculty of Medicine, Tel Aviv University, Tel Aviv 69978, Israel.

[17] Department of Physiology and Pharmacology, Sackler Faculty of Medicine, Tel-Aviv University, Tel-Aviv 69978, Israel.

[18] The Smoler Proteomics Center, Technion, Haifa 32000, Israel.

[19] Department of Dermatology, Tel Aviv Sourasky (Ichilov) Medical Center, Tel Aviv 6423906, Israel

[20] Department of Internal Medicine, Tel Aviv Sourasky (Ichilov) Medical Center, Tel Aviv 6423906, Israel

[21] School of Psychological Sciences, Tel Aviv University, Tel Aviv 69978, Israel.

[22] Robert H. Smith Faculty of Agriculture, Food and Environment, The Hebrew University, Rehovot 7610001, Israel

[23] Sagol School of Neuroscience, Tel Aviv University, Tel Aviv 69978, Israel.

[24] The Weizmann Institute of Science, Rehovot 7610001 Israel.

[25] Department of Developmental Biology and Cancer Research, Institute of Medical Research Israel-Canada, The Faculty of Medicine, The Hebrew University of Jerusalem, Jerusalem 9112102, Israel.

* Equal contribution authors: Danna Sheinboim (D.S.), Shivang Parikh (S.P.), and Paulee Manich (P.M.)

‡ Corresponding authors. Carmit Levy, carmitlevy@post.tau.ac.il (C.L.); Yftach Gepner, gepner@tauex.tau.ac.il (Y.G.); Mehdi Khaled, MEHDI.KHALED@gustaveroussy.fr (M.K.).

ABSTRACT

Exercise prevents cancer incidence and recurrence, yet the underlying mechanism behind this relationship remains mostly unknown. Here we report that exercise induces metabolic reprogramming of internal organs that increases nutrient demand and protects against metastatic colonization by limiting nutrient availability to the tumor, generating an exercise-induced metabolic shield. Proteomic and ex vivo metabolic capacity analyses of murine internal organs revealed that exercise induces catabolic processes, glucose uptake, mitochondrial activity, and GLUT expression. Proteomic analysis of routinely active human subject plasma demonstrated increased carbohydrate utilization following exercise. Epidemiological data from a 20-year prospective study of a large human cohort of initially cancer-free participants revealed that exercise prior to cancer initiation had a modest impact on cancer incidence in low metastatic stages but significantly reduced the likelihood of highly metastatic cancer. In three models of melanoma in mice, exercise prior to cancer injection significantly protected against metastases in distant organs. The protective effects of exercise were dependent on mTOR activity, and inhibition of the mTOR pathway with rapamycin treatment ex vivo reversed the exercise-induced metabolic shield. Under limited glucose conditions, active stroma consumed significantly more glucose at the expense of the tumor. Collectively, these data suggest a clash between the metabolic plasticity of cancer and exercise-induced metabolic reprogramming of the stroma, raising an opportunity to block metastasis by challenging the metabolic needs of the tumor.

Significance: Exercise protects against cancer progression and metastasis by inducing a high nutrient demand in internal organs, indicating that reducing nutrient availability to tumor cells represents a potential strategy to prevent metastasis.

INTRODUCTION

Clinical and pre-clinical studies have demonstrated that exercise plays a role in cancer prevention, as it reduces cancer incidence (1) and recurrence (2). The effect of exercise prior to tumor detection appears to be just as effective in inhibiting tumor growth as exercise before and after tumor inoculation *in vivo* (3). This suggests that exercise provides protection from tumor development, however, the mechanism underlying this preventative effect has yet to be elucidated (4,5).

Clinically, it has been suggested that exercise can have an antitumor effect through the regulation of the metabolic profile by increasing the body's insulin sensitivity thus contributing to glucose homeostasis (6), decreasing sex-steroid hormone levels (7), ameliorating the immune response (8) including reduction of inflammation (9), or secretion of skeletal muscle myokines which inhibit tumor growth (10). However, whether these modifications contribute to the protective effect of exercise is unclear.

Following exercise, skeletal muscles' metabolic adaptations are due to its increased energy demands (11,12) and include the regulation of energy and glucose-insulin-related pathways by myokines, hepatokines and adipokines (12), secreted by skeletal muscle, liver, and adipose tissue, respectively, upon exercise (12). For example, myokine interleukin 6 (IL-6) increases lipid metabolism and glucose generation in hepatocytes and improves insulin secretion from the pancreas (13).

Similarly, metabolic alterations in cancer cells are a prominent hallmark of tumor progression (14) which are determined by cell-intrinsic characteristics such as tissue of

origin (15), genetic mutations (16), and disease stage. Aerobic glycolytic metabolism of cancer cells, known as the Warburg effect, reflects a tumor's intrinsic ability to alter its metabolism (14,17), through the significant increase of its glucose uptake, allowing cancer to proliferate uncontrollably via increased anabolic processes, producing the carbon necessary for proliferation (18). In addition to intrinsic changes, tumor interactions with its microenvironment also have an impact on cancer metabolism (17). For example, the microenvironment provides metabolites, as was shown with cancer- associated fibroblasts that secrete lactate, pyruvate, ketone bodies (19), glycogen (20), and cytokines (21) and can transfer mitochondria to cancer cells (21), enhancing cancer cell mitochondrial function, tricarboxylic acid cycle (TCA) activity, oxidative phosphorylation (OXPHOS) (22), and glycolysis (20) which, together with extracellular matrix remodeling (23), leads to increased metastatic ability. Likewise, in ovarian cancer, lipids are transferred from adipocytes to tumor cells, promoting OXPHOS (24).

Given the metabolic plasticity observed during cancer progression and the metabolic alterations in host organs following exercise (11–14,17,19,20,25,26), we speculate that these two metabolic programs are clashing. We therefore hypothesize that exercise-induced metabolic reprogramming of organs transforms them into metastatic-resistant metabolic microenvironments by limiting nutrient availability to the cancer cells thus creating a metabolic-shield.

To address these hypotheses, we subjected organs from active and sedentary mice to proteomic analysis, primary cell metabolic capacity tests, including mitochondrial activity and glycolytic function, and glucose uptake analyses of primary cells to reveal metabolic reprograming towards increased catabolic processes in the

lungs, lymph nodes, liver, and muscle. We then performed a comparative proteomic analysis of plasma collected from routinely active female and male subjects before and after exercise that demonstrated a similar metabolic shift. Further, analysis of 20 years' worth of follow-up data on a prospective human cohort (n=2,734 (1302 females and 1432 males)) revealed that high intensity exercise significantly reduces the risk of metastatic cancer. To understand how these findings directly affect cancer progression, we established *in vivo* mouse models of forced exercise via treadmill running both prior to and post tumor initiation. We observed a significant reduction in melanoma dissemination into lungs, lymph nodes, and liver compared to sedentary (control) animals, in both models. Our results suggest that because exercise was performed prior to cancer initiation, exercise is altering the host organs metabolic abilities, thus protecting them against cancer dissemination. Rapamycin treatment of active stroma abolished its metabolic advantage, allowing for melanoma growth, *ex-vivo*. We then show that the stroma from active mice have a higher metabolic capability than the adjacent melanoma, whereas the stroma of control mice demonstrated the opposite trend. This suggests that the cancer-stroma crosstalk induced by exercise directly influences the tumor microenvironment therefore altering the metabolic capabilities of metastatic tumor cells. Based on our data, we hypothesize that exercise reprograms the tumor microenvironment via the development of a stromal metabolic-shield which protects the stroma from metastatic colonization by challenging cancers metabolic demands.

MATERIALS AND METHODS

Human study population.

The dataset was a population-based cohort that constituted a random sample of the Israeli general population between the ages of 25-64. The total study population included 2,734 participants; 243 new cancer cases were recorded during the 20-year follow-up period. The data was collected by the Israel Center for Disease Control and the Nutrition Department of the Israeli Ministry of Health. As our focus was on the relationship between exercise and cancer, we used a propensity score of multinomial logistic regression to control for key variables in the diet assessed using a validated questionnaire. Schematic representation of all the experimental models of human used in this study appears in Supplementary Fig. S5.

SEER classification. Each cancer case was classified according to the SEER summary stage 2000, according to the following scale: 0 – in situ; 1 – localized only; 2 – regional by direct extension only; 3 – regional lymph nodes involved only; 4 – regional by both direct extension and lymph node involvement; 7 — distant sites(s)/node(s) involved. Of the 243 subjects with cancer, 95 cancer cases had no SEER informationand were excluded from the analyses.

Exercise assessment questionnaire. The participants responded to two sets of questions from The Physical Activity Questionnaire, that aimed to assess exercisehabits such as the frequency of exercise (times per week) and the average amount of time spent on that activity. The first set of questions were asked regarding vigorous activity and the second set was asked about moderate activity that lasted for a minimum of 10 minutes. Exercise habits during leisure time were determined by a set of two questions. Participants reported the frequency (times per week) and average time they devoted to each of the following activities: walking outdoors or on a treadmill, jogging, swimming, bike riding or stationary cycling, light exercise (i.e. yoga, the Feldenkrais method, the

Alexander technique, light gymnastics), body shaping, and strength training; an “other activity” option was also offered. Based on reported total weekly time of exercise and modalities intensity, participants were classified into intensity categories according to the official American College of Sports Medicine guidelines (27). Individuals with a history of cancer at baseline were excluded from the study. Data on the date of diagnosis and the diagnostic code, assigned according to the International Classification of Diseases for Oncology, Third Edition, regarding only primary cancers (i.e., non-metastatic), were obtained, and thereby incident as well as previous cases of all-site cancer were identified (codes C00.0-C80.9).

Human cohort of steady state intensity

Population

Fourteen apparently healthy, recreationally active male and female runners between the ages of 25-45 years of age were recruited to participate in this study. All participants performed endurance exercise on a weekly basis and were familiar with running exercise. Exclusion criteria included smoking, prescribed medications, or a self-reported history of chronic pulmonary, cardiac, metabolic, or orthopedic conditions. Their physical characteristics weight (kg), height (cm), steady state heart rate (beats/min) and running pace (km/h) are shown in Supplementary Table S4. The subjects were instructed to avoid caffeine consumption for 12 h, food consumption for 3 h, and strenuous physical activity for at least 24 h prior to arrival at the laboratory for testing.

Steady state running protocol

Participants performed 30 minutes of steady state running on a motorized treadmill (Saturn 100/300, h/p/ cosmos, Nussdorf-Traunstein, Germany) using an individualized protocol. Speed determined by the highest speed that each participant can persist in for

30 minutes. Ventilator and metabolic measurements were collected during the graded protocol using breath-by-breath analysis (Quark Cardiopulmonary Exercise Testing, Cosmed, Rome, Italy) while subjects breathed through an oro-nasal facemask (7450 Series, Hans Rudolph, Kansas City, MO, United States). Heart rate (HR) was continuously monitored using a chest strap (Garmin®, model Acc, HRM-Dual, Kansas City, MO, United States).

Plasma extraction from the human cohort

Blood samples were collected for analysis prior to and immediately after the exercise. For serum extraction, blood was allowed to sit at room temperature for 1 h and then centrifuged at 1200 g for 10 minutes at 4°C. For plasma isolation, blood was placed in EDTA coated tubes (BD biosciences) and centrifuged for 15 minutes twice at 1200 xg at 4°C. The serum or plasma fractions were stored in -80 ºC until further downstream experiments.

Human RNA seq data analysis

Human Melanoma gene signature

RNA-sequencing gene expression from melanoma cancer patient (different stages and metastatic tissues) were obtained from The Cancer Genome Atlas (TCGA) and from the National Center for Biotechnology Information (NCBI) Gene Expression Omnibus (GEO) repository. Heatmap of the normalized expression of genes (rows) that are separated between the in-situ group (benign nevi, atypical nevi, vertical growth phase melanoma (VGP) and in situ melanoma) compared to metastatic melanoma, denoted the disseminated group (lung to spleen) are shown in Supplementary Table S3. Color-coding represents high expression, red, and low expression, blue, respectively. Melanoma metastatic genes were subjected for KEGG enrichment using WebGestalt

tool.

Cell culture

Ret-melanoma cells were cultured in RPMI (Biological Industries) supplemented with 10% FBS and 1% penicillin/streptomycin/L-glutamine (Biological Industries). *Ret*-melanoma stable cell line was generated by transfecting PLKO-mcherry-luc-puro plasmid (Addgene) using the jetPEI - DNA transfection reagent (Polypus) and after 48 h the stable clones were selected using the mammalian selection marker puromycin (Sigma-Aldrich, 10 µg/ml). The selected clones were expanded to be used for the experiments.

Mouse housing and exercise training

Mice

All animal experiments were performed in accordance with the guidelines of the Tel Aviv University Institutional Animal Care and Use Committee with institutional policies and approved protocols (IACUC permit: 01-15-086 and 01-19-003). All mice were housed in individually ventilated cages (IVC) in reverse light with 22+1^{o} C temperature and 32-35% humidity with *ad libitum* water and food unless mentioned the experiments. Six-week- old C57BL/6JRccHsd female mice (Envigo) were habituated for 12 days prior to experiment initiation. Schematic representation of all the experimental models of mice used in this study appears in Supplementary Fig. S5.

Exercise training

Female mice were chosen based on their increased metabolic response to exercise compared to males (28). One group of mice served as control. The other group was subjected to an exercise training protocol, modified from previously described (29). Mice were exercised every other day for the indicated time. Every day prior to the start of the exercise, mice were habituated in the experimental room for 20 minutes. On the first

day, following the lighting habituation, mice were habituated on the treadmill (Panlab Harvard Apparatus) for 10 minutes and at a speed of 5 cm/s. From day 2 and beyond, the mice were habituated in the experimental room for 20 minutes followed by treadmill exercise starting 18 cm/s for 5 minutes, increasing the speed at 2 cm/s until 24 cm/s was reached and then sustained for 8 minutes. The speed was gradually decreased by 2 cm/s every minute until 18 cm/s. Total duration of the exercise session was 20 minutes per mouse. Following the exercise, the mice were returned to their homecages.

Tumor cell injections and tumor excision

Schematic representation of all the melanoma experimental models of mice used in this study appears in Supplementary Fig. S5.

Subdermal injection: An aliquot of $1.5x10^5$ low-passage (< p15) *Ret*-melanoma mCherry–Luciferase melanoma cells were resuspended in sterile PBS (X1) and mixed at a 1:1 ratio with growth factor-reduced Matrigel (Corning) to a final volume of 50 µl. Mice were anesthetized using isoflurane, and melanoma cells were subdermally injected on the right dorsal side, rostral to the flank, with a 29G insulin syringe (BD Biosciences).

Intra-carotid injection: Mice were deeply anesthetized using intraperitoneal injection of ketamine (100 mg/kg) and xylazine (10 mg/kg). $5X10^4$ *Ret*-melanoma mCherry–Luciferase melanoma cells suspended in 50 µl saline were injected into the internal carotid artery using ultrasound guidance.

Intra-splenic injection: Mice were deeply anesthetized using intraperitoneal injection of ketamine (100 mg/kg) and xylazine (10 mg/kg). A small incision was made next to the spleen, and $1X10^5$ *Ret*-melanoma mCherry–Luciferase melanoma cells suspended in 100 µl PBS were slowly injected into the exposed hemi-spleen while the syringe was kept upright. The spleen and incision were sutured using Vicryl thread (Ethicon).

Tumor volumes were measured by caliper three times per week every other day. The tumor volume was calculated using the formula $X2 \cdot Y \cdot 0.5$ (*X*-smaller diameter, *Y*-larger diameter). Tumors were excised when they reached a volume of 1 cm^3. For the excision, ketamine (100 mg/kg) and xylazine (10 mg/kg) were used as anesthetics. The incision was made medial to the tumor. Tumors were detached with margins, to prevent their recurrence. The incisions were then closed with Vicryl threads (Ethicon).

Single-cell preparation

Lungs, lymph nodes, livers, and skeletal muscles (gastrocnemius) were harvested from mice following the indicated treatments. Organs were washed with PBS and separated into single cells. Liver tissue was minced and filtered through a 70-μm cell strainer (Corning). The other tissues were minced and incubated at 37 °C for 25 minutes in serum-free DMEM containing collagenase IV (Worthington) and deoxyribonuclease I (Worthington). DMEM supplemented with 10% FCS was used to stop the enzymatic reaction. The cell suspension was filtered through a 70-μm cell strainer (Corning). The cells were then centrifuged for 5 minutes at 500 xg at 10 °C. The pellet was reconstituted in Red Cell Lysis Buffer (Sigma-Aldrich) according to manufacturer's protocol. The tissue-derived single cells were counted and subjected to further assessments.

Glucose uptake assay

For glucose uptake analysis by FACS, cells of lymph nodes, lungs, liver, and skeletal muscles from healthy mice were washed three times with PBS, resuspended in 250 μl glucose-free DMEM (Biological Industries), and starved for 30 minutes. The green fluorescent glucose analog 2-NBDG (ThermoFisher Scientific, 100 μM) was added to the cell suspension and incubated for 30 minutes. Cells were immediately examined by

FACS on a BD FACSAria™ Fusion Cell Sorter. 2-NBDG was detected using filters designed to detect fluorescein (excitation/emission = 465/540 nm).

Lungs and lymph nodes were taken from intra-carotid-injected control and active mice and dissociated into single cells. A single-cell suspension containing a mixed population of melanoma and stromal cells were incubated in glucose-free DMEM (Biological Industries). After 30 minutes, 2-NBDG (ThermoFisher Scientific, 100 μM) was added to the media. After another 30 minutes of incubation, the mixed population was sorted to into cancer cells and stromal cells based on mCherry red fluorescence of melanoma cells using the BD FACSAria™ Fusion Cell Sorter. Green fluorescence of 2-NBDG was detected to quantify glucose uptake.

***In-vivo* bioluminescent assays**

A fresh stock solution of D-Luciferin, potassium salt (Biovision) was prepared at 15 mg/ml in sterile PBS (X1) and sterilized through a 0.2-μm filter. Mice were injected intraperitoneally with 150 mg luciferin/kg body weight 10-15 minutes prior to imaging. Mice were placed on a dark surface and imaged using a Biospace photon imager. After acquisition, a photographic image was taken.

Glycolysis and oxidative phosphorylation assays

Extracellular acification rate (ECAR)

Glycolysis in same number of live cells was measured using the XF Glycolysis Stress Test kit according to the manufacturer's instructions (Agilent). The glycolysis kit directly measures ECAR and evaluates the glycolytic flux. In brief, cells originating from the muscle or liver were seeded on wells of XF96 microplates coated with collagen1 (BD Biosciences). Cells originating from the lungs were seeded on wells coated with poly-d-lysine (Sigma-Aldrich), and cells originating from the lymph nodes were plated on wells

coated with gelatin (Sigma-Aldrich). Cells were plated at $3x10^4$ cells/well 24–48 h prior to the assay. Total RNA was extracted using the RealTime Ready Cell Lysis Buffer (Roche) and subjected to qPCR. ECAR values were normalized to *Gapdh* mRNA in each sample.

Oxygen consumption rate

The oxidative phosphorylation kit measures key parameters of mitochondrial function by directly measuring the oxygen consumption rate (OCR). In brief, same number of cells originating from the muscle or liver were seeded on collagen1 (BD Biosciences)-coated wells of XF96 microplates. Same number of cells originating from the lung were seeded on poly-d-lysine (Sigma)-coated wells, and cells originating from the lymph were plated on gelatin (Sigma)-coated wells. Cells were plated at 30,000 cells/well 24–48 h prior to the assay. Total RNA was extracted using "RealTime ready Cell Lysis Buffer" (ROCHE) and subjected to qPCR. ECAR and OCR values were normalized to *Gapdh* mRNA for each sample. Each data point represents mean ± SD (n > 4).

RNA purification and quantitative RT-PCR

Extracted RNA was quantified and its quality was assessed by measuring the 260 nm/280 nm ratio. For the mRNA measurements following Trizol (Invitrogen) isolation, cDNA was first produced using 500 ng RNA and cDNA SuperMix (QuantaBio) and then subjected to qRT-PCR using Blue SYBR low Rox (PCR Biosystems) and qRT-PCR primers. For the mRNA measurements following extraction using the RealTime ready Cell Lysis Buffer (Roche), RNA was directly subjected to one-step qRT-PCR and reverse transcriptase (Invitrogen) was added to the SYBR mix. mRNA levels were normalized to endogenous *Hprt*, *Rplp0*, or *Gapdh*. The qRT-PCR primers used are listed in Supplementary Table S5.

Mitochondria membrane potential measurement

Mitochondrial membrane potential was assessed with Tetramethylrhodamine Ethyl, Ester (TMRE; Thermo Fisher) dye. Murine primary single cells from control or active animals (lungs, lymph nodes, liver, and muscle), were incubated with a final concentration of 100 nM Rapamycin for 30 minutes in the CO2 incubator. After washing three times with complete medium to get rid of the non-specific dye. The cells were subjected to FACS analysis to determine the active and inert mitochondria in the cells at 561/610 nm.

Co-culture assay

Immunofluorescence

$1x10^5$ primary cells from the active and control groups were seeded in 24-well plates. After 24 h, $1x10^4$ of *Ret*-melanoma mCherry–Luciferase melanoma cells, were seeded on top of the primary cells. Following overnight incubation, cells were washed once with PBS and fixed using 4% paraformaldehyde (Electron microscopy sciences). Samples were scanned at 20X magnification using a Nikon fluorescence microscope, and the mean fluorescence intensity of mCherry was measured using ImageJ software. For the flow cytometry analysis, primary and melanoma cell cultures were suspended in PBS with 1% FBS (Biological Industries) and 5 mM EDTA; the red fluorescent cells were quantified out of the total population for each cell type.

Mitochondrial potential

For FACS, $1x10^6$ primary cells from active and control groups were seeded in 6-well plates. After 24 h, $1x10^5$ of *Ret*-melanoma cells labeled with PKH67 Green Fluorescent Cell Linker Kit (Sigma-Aldrich), were seeded on top of the primary cells. Following overnight incubation, cells were centrifuged at 400 g for 10 min and stained with the TMRE (Invitrogen) as per the manufacturer's protocol. After thoroughly washing three

times to remove unbound dye residues, samples were subjected to FACS analysis. Singlets were gated based on $DAPI^-$ (live cells), GFP^+ (melanoma) and GFP^- cells (primary lung cells) for mitochondrial activity. The number of active and inert mitochondria was calculated.

Proliferation

For FACS, $0.02x10^6$ primary cells from active and control groups were seeded in 96-well plates with same amount of*Ret*-melanoma mCherry cells labeled with CFSE (Biolegend), were seeded on top of the primary cells. Following overnight incubation, cells were subjected to FACS analysis. Singlets were gated based on $DAPI^-$ (live cells), $mCherry^+GFP^+$ (melanoma cells) and $mCherry^+GFP^-$ cells (melanoma proliferated) for proliferation. The percentage of the $mCherry^+$ cells denoted as proliferated was calculated from the gated cells.

Apoptosis

For FACS, $0.02x10^6$ primary cells from active and control groups were seeded in 96-well plates with same amount of *Ret*-melanoma mCherry cells were seeded on top of the primary cells with CellEvent™ Caspase-3/7 Green Detection Reagent (Invitrogen). Following overnight incubation, cells were subjected to FACS analysis. Singlets were gated based on $DAPI^-$ (live cells), $mCherry^+GFP^+$ (apoptotic melanoma cells) and $mCherry^+GFP^-$ cells (non-apoptotic melanoma cells) for apoptosis. The percentage of the $mCherry^+GFP^+$ or $mCherry^+GFP^-$ cells shown for the apoptosis were calculated from the gated cells.

Long co-culture experiment

For the direct co-culture was incubated up to 120 hours and analyzed by Incucyte ®. The intensity of $mCherry^+$ melanoma cells were calculated using ImageJ.

Hematoxylin and eosin staining

Mouse tissues were fixed with 4% paraformaldehyde at 4°C, dehydrated in a graded ethanol series, and embedded in paraffin wax. The fixed tissues were sliced into 10-µm sections and dried overnight in 37 °C. Sections were stained with hematoxylin (Sigma-Aldrich,) and eosin (Sigma-Aldrich) and mounted with DPX Mountant (Sigma-Aldrich), according to the manufacturer's instructions, and imaged at 20X magnification with a Nikon bright field microscope.

Immunohistochemistry analyses

Mouse tissues were fixed with 4% paraformaldehyde at 4°C, dehydrated in a graded ethanol series, and embedded in paraffin wax. The fixed tissues were then sliced into 10-µm sections and dried overnight in 37°C, followed by de-paraffinization in xylene and hydration in a graded series of ethanol. After microwaving in sodium citrate buffer (pH 6.0) for antigen unmasking, tissue samples were blocked with 5% BSA, 0.5% Tween-20 in PBS and then incubated with antibodies to GLUT1 (Abcam, ab40084), S100-beta (Abcam, ab52642), Complex I (Abcam, ab109798), and aldolase A (Santa Cruz Biotechnology, sc-377058), followed by incubation with fluorophore-conjugated secondary antibodies Alexa Fluor 488 (Invitrogen, A11008) and Alexa Fluor 594 (Invitrogen, A21203). Nuclear staining was performed with DAPI (Vector Laboratories). Images were obtained at 40X magnification using a Nikon fluorescence microscope. For intensity quantification, 40X images were captured and the stoma and tumor regions were marked; at least 15 areas were quantified per image (stroma or tumor), taken from at least three different tissue samples from each mouse. Fluorescence images were split into separate channels and converted into 8-bit images using ImageJ software. A specific area in each image was subjected to quantification using the ROI manager function to

precisely quantify the intensity from the same place in different channels simultaneously; each intensity was normalized to DAPI from the same image to rule out discrepancies due to differences in cell numbers. We performed *t*-tests for each target (GLUT1, S100, ALDOA, and Complex 1) within and between areas (stroma and tumor) for homoscedastic or heteroscedastic analyses.

Proteolysis and mass spectrometry analysis

Human plasma or mouse internal organs after perfusion were subjected to a mass spectrometry (MS) analysis for the small proteins as previously done by us(30). Proteins from 10-µl aliquots of serum in 8 M urea were separated using a Microcon 30- kDa Centrifugal Filter Unit (Millipore). The resultant proteins were reduced with 3 mM DTT in 8 M urea and 400 mM ammonium bicarbonate (60 ºC for 30 minutes), modified with 12 mM iodoacetamide (in the dark, room temperature for 30 min) and digested in 1 M urea, 50 mM ammonium bicarbonate with modified trypsin (Promega) at a 1:50 enzyme-to-substrate ratio, overnight at 37 ºC. The tryptic peptides were desalted through C18 TopTips (Glygen), dried, and re-suspended in 0.1% formic acid. The peptides were resolved by reverse-phase chromatography on 0.075 X 180 mm fused silica capillaries (J&W) packed with Reprosil reversed-phase material (Dr. Maisch HPLC GmbH). The peptides were eluted with a 120-min linear gradient of 5% to 28%, 15 minutes linear gradient of 28% to 95%, and then 25 min at 95% acetonitrile with 0.1% formic acid in water at a flow rate of 0.15 µl/minutes. Mass spectrometry was performed with a Q Exactive HF mass spectrometer (Thermo) in a positive mode using repetitively full MS scan followed by collision-induced dissociation of the 20 most dominant ions selected from the first MS scan. The mass spectrometry data from from each sex (n = 3 males and n = 3 females) in the human cohort or from the indicated organs from eight mice (four in

the active group, four in the control group) were analyzed using the MaxQuant software 1.5.2.8 and the human or mouse proteome from the Uniprot database (31) with 1% FDR (false discovery rate). The data were quantified by label-free analysis using the same software. Statistical analysis of the identification and quantization results was done using Perseus 1.6.10.43 software (32). Proteins were evaluated for KEGG pathway enrichment using the Proteomaps too and the GO functional annotation tool (33). For human the differential expression of proteins after mass spec analysis appears in Supplementary Table S2. For mouse, the up-regulated proteins in control (indicated in red) and active (indicated in blue) after mass spec analysis appears in Supplementary Table S1.

Membrane labeling the melanoma cells

Naïve *Ret*-melanoma cells were labeled either with mCherry (PKH26) or GFP (PKH67) cell membrane labeling dye (Sigma-Aldrich) following the manufacturer's instructions.

Inhibiting the cellular metabolism using the Rapamycin

Murine primary cells from control or active animals (lungs) incubated with the final concentration of 100 nM mTOR inhibitor - Rapamycin (GoldBio) for 3 hours in the CO_2 incubator followed by washing with complete culture medium.

TMRE with and without rapamycin:

For TMRE experiments, following the rapamycin treatment the murine lung cells, were stained to check the mitochondria membrane potential measurement using the TMRE as mentioned above followed by FACS analysis.

Melanoma survival with and without rapamycin:

Ret-melanomas' ability to survive in different primary cell environments was measured via FACS. Naïve *Ret*-melanoma cells were labeled with PKH26 and $0.05X10^6$ cells

were seeded into 24-well culture plates. Single-cell preparations from the lungs of control and active mice were performed and $0.05X10^6$ cells from each group were treated with or without rapamycin (vehicle) and stimulated for 3 hours in the CO_2 incubator. The rapamycin or control-treated cells were directly co-cultured with the mCherry labeled *Ret*-melanoma cells for 24 hours at 37°C and 5% CO_2. Following the incubation, trypsinized cells were subjected to FACS analysis for determining the survived melanoma cells at 465/540 nm wavelength.

Primary mouse melanoma gene expression analysis

Downregulated genes from primary melanoma obtained from B16F10 melanoma injected mice following exercise from (3) were subjected for KEGG enrichment analysis using WebGestalt.

Statistical analysis and reproducibility

All data shown as means and standard errors of the mean. We used a random experimental design. For mouse experiments, student's *t*-tests (two-tailed) for two-group comparisons were performed for the indicated conditions. For the human cohort of 20-year follow-up in Israeli general population a propensity score was constructed using a multinomial logistic regression, through which was calculated the probability of being classified into a specific physical activity category. The propensity scores weighted model (w) included the following variables as covariates: age, sex, ethnicity, neighborhood socioeconomic status, income, education, proportion of saturated fatty acids out of the total energy intake, total energy intake, total alcohol consumption, dietary fiber intake, self-rated health, anemia, osteoporosis, hypercholesterolemia, hypertriglyceridemia, diabetes, hypertension, stroke, coronary heart disease, occupational physical activity, marital status, self-definition of religious level, highest education certificate/academic

degree, employment, body mass index, smoking year. For the mass spectrometry data analyzed in the human cohort (n = 6 biologically independent humans) with 5% FDR (false discovery rate) or from the indicated organs from eight mice (n =4 from each group) with 1% FDR (false discovery rate).

Data and Materials Availability

The accession number for the MS proteomics data reported in this paper is deposited in the PRIDE repository under accession numbers: PXD035630 and PXD035648. The raw data associated with this paper can be available from the corresponding authors upon request.

RESULTS

Exercise reprograms tissue metabolism in mice

To explore the molecular changes that occur in murine internal organs following exercise, we established an *in-vivo* exercise model (Fig. 1A; Supplementary Fig. S5A; ref 29). We performed comparative proteomics analyses, by mass spectrometry, of typical metastasis host organs: lungs, lymph nodes, and livers from sedentary and active mice that were subjected to an exercise regimen for 8 weeks (Fig. 1A; Supplementary Table S1). Skeletal muscle was also analyzed, as they undergo significant metabolic changes upon exercise (34), and skeletal muscle is rarely a site for metastatic colonialization. Hematoxylin and eosin staining from lungs, lymph nodes, livers, and muscles from control and active mice are shown (Supplementary Fig. S1A). Principal component analysis (PCA) of organs from the control sedentary group were scattered, while organs from the active group demonstrated a grouped pattern, suggesting that exercise synchronizes the organ's biological properties independently of an individual's initial characteristics (Supplementary Fig. S1B). This finding suggests that the metabolic

alterations following exercise are common to all trained animals. Proteins that were found to be differentially expressed from the mass spectrometry between the active and control groups (Supplementary Fig. S1C) were subjected to KEGG analysis and Proteomaps revealing that there were metabolic shifts in tissues from active versus control mice (Fig. 1B). In active mice, there was upregulation of carbohydrate metabolism, glycolysis, OXPHOS and mitochondrial biogenesis in all tissues examined (Fig. 1B). Some of the metabolic changes were organ dependent, for example, in both lymph node and liver tissues there was upregulation of glycolysis and mitochondrial biogenesis, however, the liver uniquely exhibited enrichment in the TCA cycle.

We subjected the differentially expressed proteins to gene ontology (GO) analysis without considering expression scores and compared the overlap of all the significantly enriched pathways from each organ (Fig. 1C). This revealed that catabolic processes (defined as those with the term “GO biological process") and mitochondrial processes (defined as those with the term “GO cellular compartment") were the most enriched in the investigated tissues of active mice (Fig. 1C and D; Supplementary Fig. S1D). The blood glucose levels were the same before and after exercise in both active and control mice (Supplementary Fig. S1E), suggesting that systemic glucose homeostasis is maintained upon exercise, in line with the literature (35), and that the observed metabolic alterations following exercise are due to changes in the organs themselves.

Next, we measured the glucose uptake of primary single cells originating from the lymph nodes, lungs, livers, and skeletal muscles of active and control mice. Cells were incubated for 30 minutes in glucose-free DMEM followed by the addition of the green-fluorescent glucose analog, 2-NBDG, for 30 minutes. FACS analysis revealed significantly higher levels of 2-NBDG in cells from active lymph nodes, lungs, livers, and

skeletal muscles compared to the cells from control mice (Fig. 1E). Since glucose is the main substrate of glycolysis and of the OXPHOS cascade (22,24) as well as the major source of energy during exercise (11), we next examined glycolysis in primary cells originating from the lymph nodes, lungs, livers, and skeletal muscles of active and control mice. Glycolytic function was assessed by extracellular acidification rate (ECAR). In all the investigated tissue-derived cells from the active mice, the glycolytic function was significantly higher than in that from control mice (Fig. 1F; Supplementary Fig. S1F).

To further understand the metabolic differences between tissues from active and sedentary mice, we conducted a mitochondrial activity test. Using tetramethylrhodamine ethylamine (TMRE) (36), we analyzed the number of active mitochondria in primary cells isolated from active and control tissues via FACS. We found that primary cells originating from control mice had significantly fewer active mitochondria compared to active primary cells (Fig. 1G). This significant reduction in active mitochondria validates our proteomic analysis. Along the same line, oxygen consumption rate (OCR) measurement was significantly higher in active animals compared to controls (Supplementary Fig. S1G) as well as the expression of mitochondrial specific genes (*TFAM*, *POLRMT*, *TFB1M*, *TFB2M*, *Cyc1*, and *Mrps35*) (Supplementary Fig. S1H). Our findings are in line with previous studies that showed that skeletal muscles and liver tissues have increased mitochondrial biogenesis following exercise (37). However, to the best of our knowledge, this is the first report of an elevation in mitochondrial activity following exercise in the lymph nodes and lungs, which are not considered to be part of the direct response to exercise (37). Further, as glucose is unable to cross lipid membranes (38), glucose transporters, GLUTs, on the cell surface are critical for glucose uptake. There are multiple GLUTs, varying in expression (dependent on the cell type), in their affinities for

glucose, and in their abilities to transport fructose. GLUT1 is the most universally expressed isoform of the GLUT receptors (38). GLUT2 is expressed in the liver, kidney, and central nervous system, among others, and is important in the expression of glucose-sensitive genes. GLUT4, found in adipocytes, is stimulated by insulin levels thus enhancing insulin sensitivity and glucose uptake (39). By using these four GLUT receptors as our panelfor checking GLUT expression in mouse tissues after exercise, we were able to get a well-rounded perspective from GLUTs differing in cellular locations and environmental triggers. We found that expression levels of *Glut1*, *Glut2*, and *Glut4* mRNAs, which exclusively transport glucose (38), were significantly higher in cells from the active mice compared to control mice (Fig. 1H), which is line for GLUT1 and GLUT4 expression in skeletal muscle post-exercise (40). Taken together, these data indicate that exercise causes metabolic reprogramming of various organs, creating a new microenvironment throughout the body.

High-intensity exercise significantly reduces the risk of highly metastatic cancers in humans

To examine the observed metabolic reprograming in mice upon exercise in humans, we performed a plasma proteomic analysis (Supplementary Table S2). Using six subjects from a cohort of healthy, routinely active people (3 female, 3 male), we collected blood samples before (following 48 hours of rest) and after they ran on a treadmill at high intensity (75% Heart Rate) for 30 minutes (Fig. 2A; Supplementary Fig. S5B). GO analysis of the upregulated proteins following the exercise session revealed a significant enrichment in the IGF-I pathway in all subjects (Fig. 2B and C; Supplementary Fig. S2A). Like insulin, IGF-I promotes glucose uptake via the translocation of glucose transporterssuch as GLUT1 and GLUT4 to the cell membrane (38,41). Further,

in a separate cohort of fourteen subjects who ran at RER above 0.95 (high-intensity), we found that fat-to-carbohydrate turnover (i.e., the ratio between glucose and fat utilization during exercise) is affected by exercise intensity, with glucose utilization rising in prominence as the intensity of exercise increases (Fig. 2D; Supplementary Fig. S5C). Therefore, the IGF-related pathway regulating glucose homeostasis (41) from the first cohort, is supported by the increased usage of carbohydrates (11) following high-intensity exercise of the second cohort.

Although metastases are the major cause of cancer mortality (14), most human epidemiological studies that have studied the role of exercise in cancer outcomes have not considered the stage of the cancer at diagnosis, the intensity of the exercise, and the interaction between the two. To investigate this relationship, we examined a prospective cohort (n=2,734 (1302 females and 1432 males)), that was followed for 20 years, with self-reported duration and intensity of exercise (Supplementary Fig. S5D). Data on exercise was obtained via a personal interview at baseline, based on a standard questionnaire (42,43) (further details can be found in Materials and Methods). The cohort study was linked to the Israel National Cancer Registry via their national identification numbers. The registry covers the entire Israeli population, with 97% estimated completeness of ascertainment for solid tumors (44), whereas all cases of malignant neoplasms, carcinoma in situ and high-grade intraepithelial neoplasia, and benign neoplasms of the brain and central nervous system have been recorded (45).

Our analysis revealed that exercise tends to lower the risk of developing cancer in both men and women, with a greater association on highly metastatic cancers (SEER 7) (Fig. 2E). Specifically, high-intensity exercise significantly reduced the incidence of highly metastatic cancers (73% risk reduction compared to the inactive group, $p<0.05$);

(Fig. 2E and F). This implies that high-intensity exercise may prevent cancer dissemination to distant sites. Our epidemiological study illustrates the unique and significant interaction between exercise intensity and metastatic cancer development in humans.

This data suggests that our originally cancer-free participants had a reduced likelihood of highly metastatic tumor formation. Additionally, routinely active females and have shifted their macronutrient utilization and enrichment of metabolic pathways, leading us to hypothesize that exercise is inducing systemic changes that are protecting against tumor development in humans.

Exercise inhibits melanoma metastasis formation in mice via metabolic-shield

To evaluate the potential protective role of exercise-induced increased metabolic ability of lymph nodes, lungs, and livers against metastasis formation, we established a mouse cancer model in which we tested the effects of exercise (Supplementary Fig. S5E). Since cutaneous melanoma has a high probability of metastatic dissemination to most organs, including the lymph nodes, lungs, and liver, we used this cancer as our model. To follow tumor growth and spread, we used a murine *Ret*-melanoma cell line derived from a spontaneous melanoma in *Ret*-transgenic mice, which was engineered to carry mCherry and luciferase reporters (Supplementary Fig. S3A and B). We used a forced treadmill running protocol, which enabled us to gradually increase exercise intensity (5). Mice were divided into a sedentary group (control) and a group subjected to the exercise protocol (active); each group contained at least 3 mice. The active group was subjected to a training protocol (29) for 8 weeks prior to sub-dermal injection of *Ret*-melanoma mCherry–Luciferase melanoma cells; after 4 days of recovery, the exercise regimen was continued for up to 4 additional weeks (Fig. 3A).

We found a significant reduction in the active group's primary tumor volume compared to tumors in the control group at the end of the second exercise period (Fig. 3B), which is in accordance with a previous study (3). We then investigated metastasis formation after excision of the primary tumor. This pre-clinical model enables spontaneous metastasis formation, which allows us to trace the multi-step process of metastasis. The primary tumors were excised when they reached 1 cm^3 in size. Mice were then given 10 days to recover before continuing with the training protocol. 4 weeks post primary tumor excision training was finished, a metastasis examination was completed (Fig. 3A). We then isolated single cells from the lymph nodes, lungs, and liver, and sorted melanoma cells from stromal cells based on *Ret*-melanoma stably expressing mCherry fluorescence. The number of melanoma cells were significantly reduced in the lungs and liver and a reduced trend in the lymph nodes of the active group compared to the control group (Fig. 3C). These results indicate that exercise inhibits both primary tumor growth and spontaneous metastasis formation.

Since the primary tumor volumes were significantly smaller in the active group than the control group (Fig. 3B), we reasoned that the number of circulating melanoma cells was decreased and thus the number of cells available for metastasis formation would be limited in the active group. Taking this into consideration, we implemented a model, specifically for metastatic formation, that bypasses the stage in which melanoma cells invade into the dermis for metastasis formation. By using intra-carotid injection of *Ret*-melanoma mCherry–Luciferase melanoma cells (targeting the lymph nodes and lungs) or intra-splenic injections (targeting the liver), we evaluated whether exercise performed pre and post tumor injection had a protective effect against metastases (Fig. 3D). *Ex-vivo* examination of the metastases showed a significant reduction in

bioluminescence in the lungs (Fig. 3E; Supplementary Fig. S3C) as well as in the lymph nodes and liver in the groups of mice that were exercised pre and post injection of tumor cells compared to control mice (Supplementary Fig. S3D and E). The expression of *mCherry* and melanoma markers *Mlana* and *Tyrp1* (34) were significantly lower in the lungs (Fig. 3F) as well as lymph nodes and livers (Supplementary Fig. S3F) of mice exercised pre and post tumor cell injection. This indicates that exercise pre and post tumor inoculation has a significant protective effect against metastasis formation.

To understand this protective effect of exercise and separate it from the effect of the tumor and stroma together, we altered our model to training exclusively prior to the *Ret*-melanoma mCherry–Luciferase melanoma injection (herein “pre”; Fig. 3D; Supplementary Fig. S5F). In this model, there was significantly reduced bioluminescence in mice exercised only pre tumor cell injection compared to control mice (Fig. 3G). The expression of *mCherry*, and melanoma markers *Mlana*, and *Tyrp1* were significantly lower in the lungs of the mice exercised pre tumor cells injection than the controls (Fig. 3H). These results suggest that exercise has a protective effect against metastatic dissemination due to changes in the microenvironment prior to tumor arrival.

We then examined whether exercise could inhibit cancer formation *ex-vivo*. Single cells were isolated from the lymph nodes, lungs, and livers of control mice and active mice that were not injected with melanoma. These primary cells were then co- cultured with *Ret*-melanoma cells for 24 hours (Fig. 3I; Supplementary Fig. S5G). The number of *Ret*-melanoma cells that survived during the experiment were significantly reduced when co-cultured with cells that originated from organs of active mice compared to those from control mice, as shown by microscopy (Fig. 3J; Supplementary Fig. S4D) and by FACS (Fig. 3K). Interestingly, melanoma cell proliferation was significantly reduced in

the presence of primary lung cells from active mice compared to controls while no significant changes in proliferation were observed when in culture with liver and lymph nodes cells (Supplementary Fig. S3G, left panel). On the other hand, melanoma apoptosis showed an opposite trend (Supplementary Fig. S3G, right panel), indicating that active stroma may affect either melanoma proliferation or survival, in a context dependent manner.

Our findings thus far have pointed us towards metabolic alterations being a key player in making active tissues a hostile microenvironment for melanoma. To test this, we targeted the metabolic abilities of these cells directly with rapamycin, blocking the mTOR pathway (46), to see if the protection against cancer progression can be reversed. To ensure that rapamycin is in fact affecting the metabolism of the primary cells, we used TMRE to test the mitochondrial activity in primary cells with and without rapamycin treatment. We saw that 3-hour treatment with rapamycin significantly reduced the number of active mitochondria in primary lung cells from active mice (Supplementary Fig. S3H and S4E). We then tested if melanomas survival rate was affected by the change in the metabolism of the primary cells. We saw that melanoma that was co- cultured overnight with rapamycin treated primary cells survived and proliferate better than that in culture with untreated primary cells (Fig. 3L; Supplementary Fig. S3I).

Put together, these results imply that exercise reduces primary melanoma volume and metastatic dissemination into lymph nodes, lungs, and liver. The creation of a metabolic-shield via the reprogramming of key metabolic characteristics of these organs results in a tumor microenvironment that does not support tumor cell colonization and therefore provides a systemic protective effect.

Exercise induces metabolic crosstalk between the tumor and its

microenvironment *ex vivo*

One of the key hallmarks of cancer progression is its ability to make metabolic alterations, including enhanced tumor aerobic glycolytic metabolism, termed the Warburg effect (14). We performed a gene expression clustering analysis of melanoma, organized according to stage of progression, from benign nevi to metastasis, in various organs (Supplementary Table S3). This analysis revealed two distinct gene signatures related to primary versus metastatic human melanoma (Fig. 4A, left panel; Supplementary Fig. S4A). GO analysis of these genes found significant metabolic enrichment (i.e. metabolism of carbon, galactose, glycine, serine, amino sugar, and nucleotide sugar) in the metastatic samples, whereas the immune-related pathways were more highly enriched in the primary tumors (Fig. 4A, right panel; Supplementary Fig. S4A), which is in line with the literature (14). Given the metabolic shift during cancer progression and the metabolic reprogramming following exercise, we reasoned that the two metabolic programs might be clashing.

We then performed an enrichment analysis based on microarray data collected in a previous study (3) and found downregulation of metabolic pathways in the primary tumors of active animals compared to tumors derived from control animals (Fig. 4B). This suggests that exercise may affect metabolism of tumor cells directly or alter it indirectly through effects on the tumor microenvironment. In the case of an indirect effect, exercise could increase the uptake of nutrients by the active stroma microenvironment, thus changing the availability of nutrients to tumor cells or exercise might induce stroma cells to secrete factors that affect the tumor phenotype. This type of competition, however opposite to our observations, between tumor and stroma has been previously reported in the literature through the loss of T cell function due to enhanced glucose uptake by tumor

cells leading to reduced glucose consumption of tumor-infiltrating T cells.

To evaluate how exercise challenges tumor metabolism thus affecting metastasis development, we examined the metabolism of melanoma cells and primary stoma cells from active or control mice during co-culture. Primary lung cells from control and exercised mice were co-cultured with *Ret*-melanoma cells for 24 hours followed by mitochondrial activity analysis using TMRE (Supplementary Fig. S5F). Lung stroma cells from active animals showed significant induction in mitochondrial activity compared to cells from control mice (Fig. 4C, upper panel). Interestingly, no significant difference was observed in mitochondrial activity of melanoma cells co-cultured with the stroma from active versus control mice (Fig. 4C, lower panel).

To explore whether the stroma's mitochondrial potential can affect the tumor mitochondrial activity and growth, we repeated the experiment (Fig. 4C) in the presence of mitochondria uncouplers and inhibitors of the ETC including FCCP and actinomycin D (Supplementary Fig. S2B, upper panel). No significant differences were observed in melanoma cells' mitochondrial activity; however, melanoma growth was significantly higher when cocultured with active stroma cells treated with both drugs compared to vehicle (Supplementary Fig. S2B, lower panel). This indicates that although only 50% of melanoma cells succeeded in seeding in active tissue compared to control (Fig. 3K), melanoma mitochondrial status does not affect their ability to seed in either active or control stroma.

We next evaluated glucose uptake of primary cells isolated from the metastases in the lungs and lymph nodes of the active and control mice (Fig. 4D). The cells were sorted based on the mCherry fluorescence of the *Ret*-melanoma cells, resulting in two populations: cancer cells ($mCherry^+$) and stromal cells ($mCherry^-$). Cells were then

starved for 30 minutes in glucose-free DMEM, after 30 minutes 2-NBDG was added. FACS analysis of the 2- NBDG uptake performed after 30 minutes of incubation revealed significantly higher glucose uptake of the stroma from active mice than control mice (Fig. 4E). In contrast, melanoma cells from active animals had significantly higher glucose uptake than melanoma cells from the control animals (Fig. 4E). Sorted cells from active and control mice were also subjected to mRNA analysis of *Glut4*, a marker of glucose sensing, *Aldoa*, indicative of glycolysis, and *Hspa9*, a marker of mitochondrial activity. Stromal cells isolated from active mice had significantly higher expression of these metabolic markers compared to the control stroma (Supplementary Fig. S4B). Whereas, in most instances, tumor cells from active animals expressed significantly lower levels of metabolic markers than tumor cells from control mice (Supplementary Fig. S4C). These experiments suggest that melanoma cells have less metabolic activity in tissues from exercised mice due to the high metabolic demand of the stroma in these animals.

To examine melanomas metabolic adaptation further, we subjected biopsies of lymph nodes, lungs, and livers harboring metastases from active and control mice to pathology analysis. Melanoma and stroma were defined based on distinct morphological changes seen in hematoxylin and eosin staining and on staining for melanoma-specific marker S100-beta. We also stained the tissues for GLUT1, ALDOA, and COMPLEX I. The latter takes part in the electron transport chain and is a marker of oxidative phosphorylation. To allow comparison between stroma and tumor as well as between active and control samples, intensities of GLUT1, ALDOA, and COMPLEX I were normalized to intensities of DAPI staining of the same areas. Stroma of tissues from active mice had significantly higher expression of metabolic markersthan stroma of control animals, but tumor metastases in tissues from active mice had significantly lower expression of these markers compared to metastases of control mice (Fig. 4F-H).

When comparing the metastases to its stroma, we found significantly higher expression of the metabolic markers in the tumor region compared to stroma in the control mice, whereas in the active animals we found the opposite trend (Fig. 4F-H). There were no differences in S100-beta levels in tumor area of the control and active mice, nor in the stroma area (Fig. 4F-H). Taken together, these results support our hypothesis that exercise, which increases the microenvironmental metabolic demand, resulting in a microenvironment that does not support melanoma colonization, thus protecting against metastatic spread.

DISCUSSION

Mutation, selection, and adaptation processes during cancer progression likely occur at both the primary tumor and at the metastatic site (14), however the dynamics of these processes are poorly understood. Tracking the metabolism of the tumor and its stroma might be an opportunity to reveal the dynamics of these three forces. Dupuy *et al.* suggest that different metabolic traits that characterize the heterogenous population of breast cancer cells dictates their selective preferences to disseminate to specific sitesvia specific mutations or adaptations to metastatic microenvironments that support their metabolic demands (47).

Our *in-vitro* and *in-vivo* data demonstrate that approximately 50% of the cells succeed to disseminate in active tissue, suggesting that the metastasis-host organ transformed into a more highly metabolic organ. We challenged the heterogeneous population of the primary tumor, and the ability of certain clones to “choose” their metastatic site according to their metabolic demands. This favors the selection model (14) by which cells from primary tumors metastasize to favorable metabolic niches. Of the melanoma cells that were successfully able to metastasize, we showed that

melanoma cells in active mice had reduced their metabolic needs compared to cells in sedentary mice. This suggests that metastasis development stems from interactions with the microenvironment (stromal cells, nutrients, and oxygen) (48). It is therefore clear that cancer cells metabolic state plays a central role in both selection and adaptation during cancer progression, a hypothesis that requires further investigation to determine the precise dynamics.

The classical hallmarks of cancer, including immune response, tumor vasculature, hypoxia, pH, and autophagy (14), all can be affected by exercise thus helping to further create a hostile tumor microenvironment against melanoma. We will expand here on two aspects, the immune response, and the extracellular matrix (ECM). Clinically, melanoma patients who responded to two types of immunotherapies (TIL- based or anti-PD1) had highly increased levels of metabolic proteins, mitochondrial activity, and oxidative phosphorylation (49). Further, glucose consumption by cancer cells has been shown to metabolically restrict T cell activity in the tumor microenvironment causing T cell loss of function (50). Without proper levels of glucose, mTOR activity, as well as activity of other pathways, is reduced in T cells (50). In our study, we targeted mTOR activity in the stroma and were able to significantly return active stroma cells to the control state, in terms of melanoma's ability to grow when in co-culture with treated active stroma. This supports the hypothesis that exercise may induce metabolic capabilities of the immune cells in the tumor microenvironment thus enhancing the immune response to cancer. Future studies should investigate the relationship between metabolic shifts and immune system efficacy.

Given that cancer progression and metastasis formation is comprised of many factors working together for melanoma to successfully reach the metastatic phase, we

recognize that factors such as proliferation inhibition may be at play in our model. Since we, and others (3), found that the primary tumor is smaller upon exercise we reasoned that there will be fewer circulating tumor cells and therefore less metastases, therefore we bypass this hurdle, and we injected same amount of melanoma cells inter-carotid. However, our inter-cardiac injections also showed less growth, and does not uncouple the proliferation defects from metastatic seeding defects. Further studies are required to understand the direct effect of exercise on *in-vivo* tumor proliferation separated from the tumors ability to seed in the metastatic niche.

Another aspect in tumor development is ECM remodeling of the pre-metastatic niche (23). After exercise, the intermuscular ECM is altered (23). It will be interesting to explore whether changes in ECM-related genes and proteins induced by exercise are also observed in metastatic host locations (e.g., lung, liver, lymph nodes), in addition to the muscle. We found that metabolic properties such as glucose uptake and metabolic mitochondrial activity marker expression were downregulated in melanoma cells from active mice that had metastasized to stroma. Studies have shown that dormant cancer cells have lower metabolism than non-dormant cancer cells (51), thus melanoma cells that survived in the active microenvironment may have become dormant. Interestingly, autophagy is activated during nutrient deficiency, and autophagy inhibition has been shown to result in apoptosis of dormant breast cancer cells (52). Therefore, dormancy and autophagy should be explored with our exercise animal model to understand if autophagy inhibition more efficiently induces apoptosis of metastatic cells under an exercise protocol.

Various agents have been identified which target the metabolism of either the tumor or the stroma cells of the metastatic niche (14). Some metabolic enzyme

inhibitors are currently being evaluated in clinical trials (53). Tumors can become resistant to such treatments due to their metabolic plasticity, allowing them to bypass the blockade of a specific metabolic pathway by adopting new metabolic traits (54). Thus, like combined treatments of signaling pathway inhibitors for melanoma (55), the simultaneous inhibition of multiple metabolic pathways should be evaluated (56). Moreover, it has recently been suggested that the immunotherapy resistance of melanoma patients can be overcame by combining the treatment with metabolism-related drugs (49). Here, we show that exercise reprograms the metabolic capacity of non-skeletal tissues known to be niches for metastatic melanoma as shown by the increased activity of the glycolytic pathway and increased mitochondrial activity. This suggests that exercise generates a metabolic-shield and may be beneficial in combination with immunotherapy as a replacement or in addition to metabolism-altering drugs. Although we used melanoma as our pre-clinical model since it is a highly metastatic cancer, we expect that our findings will translate to other cancers, given that our human studies were not cancer specific, and our mouse findings refer to the metabolic shift prior to cancer arrival.

Glycogen metabolism is upregulated in many tumor types, suggesting that it is an important aspect of cancer cell pathophysiology (57). Since muscle cells require a large amount of glycogen following bouts of prolonged or high-intensity exercise to return to pre-exercise glycogen concentrations, muscles may take up to 24 h to replace glycogen stores (58). This phenomenon, which is known as super-compensation, might protect muscles from metastatic dissemination since the muscle cells compete with the malignant cells for available glycogen resources. Further, the super-compensation process might also provide a metabolic shield again tumor seeding in internal organs

(59). This should be further investigated. An additional way to generate competition between normal and cancerous cells is by decreasing the available glucose resources. For example, low-carbohydrate diets, such as the ketogenic diet, have been proposed to starve malignant growth by inhibiting the availability of glycogen storage. Several long-term studies with large human cohorts and studies using animal models have shown a correlation between cancer risk and dietary composition (60). Several factors related to nutrition are associated with cancer incidence. For example, overfeeding leads to obesity (61), which is associated with impaired whole-body metabolism including a decreased ability to quickly clear and store excess calories. High levels of expression of the tumor progesterone receptor, as observed in obese humans and animals who are overfed, are associated with a glycolytic–lipogenic phenotype typical of aggressive tumors and with high metastatic rates (60). In addition, high fat diets and consumption of high amounts of saturated fatty acids increase gut permeability and induce colonic inflammation and mesenteric fat inflammation, which increase overall cancer risk (60). Other factors that are correlated with cancer risk are alcohol consumption, which is detrimental, and fiber intake, which improves cancer immunosurveillance (60). In our human cohort analysis, we controlled for these key factors in the diet to determine the independent effect of the level of exercise on cancer risk, however a future study should investigate the combination of both nutrition therapy and physical activity to limit metastatic growth.

As a final note, it will be important for clinical application to explore how long the exercise effect lasts and how long-term resting alters the dissemination of cancer cells. The existing literature is contradictory. For example, in one study, a very limited amount of strength and muscle fiber was retained after 8 weeks of detraining, while another

showed that halting training did not negatively affect muscles fibers and breathing capacity benefits due to the initial exercise regimen (62,63). Mouse studies are also contradictory, which might be due to the use of various training methods, resting periods, and measures of exercise retention, as explained in the review by Gundersen *et al*., (64). To investigate the long-term effects of exercise and subsequent resting a future study is needed. Further, since Olympic athletes and professional athletes are not immune from developing cancer, even with their high intensity training regimens (65), and exercise intensity depends on an individual's ability, proposing personalized exercise regime for each patient might provide better clinical outcomes.

Acknowledgements

C.L. acknowledges grant support from the European Research Council (ERC) under the European Union's Horizon 2020 research and innovation programmer (grant agreement no. 726225), the I-CORE Gene Regulation in Complex Human Disease Center (no. 41/11), and Israel Science Foundation (ISF) (grant 129/13).

Author contributions

D.S. designed the scientific approach and performed majority of the biological experiments and participated in writing of the manuscript. S.P. participated in all the *in-vivo* experiments and performed the immunohistochemistry and melanoma co-culture experiments and analysis and participated in writing the manuscript. P.M. performed mouse training exercise and melanoma co-culture experiments and analysis and proteomic analysis and participated in writing the manuscript. S.D. performed the glucose uptake assay. R.P. performed mouse exercise training and participated in *in- vivo* and in vitro experiments. E.S. performed the experiments. G.Y. and T.G. performed the mass

spectrometry proteomic analysis. S.L. collected the blood from human subjects for this study. R.B., E.N., G.C. and R.P. provided a useful discussion. G.C., N.G., K.C., and Y.G. analyzed the human cohort study. N.G., R.A., K.C., and Y.G. and Y.G supervised the epidemiologic data analysis. Y.G., L.K.-B., T.S., N.G., I.M., and K.C. and designed the human cohort and the intervention trial. A.L. and E.P. provided skeletal muscle cells and muscle condition media. D.B.-Z. designed the mitochondrial experiments and analysis. S.L. and Y.T. performed the differential mass spectrometry analysis. S.A.-R., and H.E.-F., participated in *in vivo* experiments. M.K. performed the stable for *Ret*-melanoma mCherry — Luciferase melanoma cells, designed and analyzed the experimental approach, and wrote the manuscript. C.L. developed the hypothesis, designed and analyzed the experimental approach, coordinated the project, and wrotethe manuscript.

Bibliography

1. Moore SC, Lee I-M, Weiderpass E, Campbell PT, Sampson JN, Kitahara CM, etal. Association of Leisure-Time Physical Activity With Risk of 26 Types of Cancer in 1.44 Million Adults. JAMA Intern Med. 2016;176:816–25.

2. Brown JC, Gilmore LA. Physical activity reduces the risk of recurrence and mortality in cancer patients. Exerc Sport Sci Rev. 2020;48:67–73.

3. Pedersen L, Idorn M, Olofsson GH, Lauenborg B, Nookaew I, Hansen RH, et al. Voluntary Running Suppresses Tumor Growth through Epinephrine- and IL-6- Dependent NK Cell Mobilization and Redistribution. Cell Metab. 2016;23:554–62.

4. Hojman P, Gehl J, Christensen JF, Pedersen BK. Molecular mechanisms linking exercise to cancer prevention and treatment. Cell Metab. 2018;27:10–21.

5. Pedersen L, Christensen JF, Hojman P. Effects of exercise on tumor physiology and metabolism. Cancer J. 2015;21:111–6.

6. Magkos F. Exercise and insulin sensitivity—where do we stand? you'd better run! US Endocrinol. 2008;04:23.

7. Ennour-Idrissi K, Maunsell E, Diorio C. Effect of physical activity on sex hormones in women: a systematic review and meta-analysis of randomizedcontrolled trials. Breast Cancer Res. 2015;17:139.

8. Koelwyn GJ, Wennerberg E, Demaria S, Jones LW. Exercise in Regulation of Inflammation-Immune Axis Function in Cancer Initiation and Progression. Oncology (Williston Park, NY). 2015;29:908–20, 922.

9. Woods JA, Wilund KR, Martin SA, Kistler BM. Exercise, inflammation and aging. Aging Dis. 2012;3:130–40.

10. McTiernan A. Mechanisms linking physical activity with cancer. Nat Rev Cancer. 2008;8:205–11.

11. Hawley JA, Hargreaves M, Joyner MJ, Zierath JR. Integrative biology ofexercise. Cell. 2014;159:738–49.

12. Murphy RM, Watt MJ, Febbraio MA. Metabolic communication during exercise. Nat Metab. 2020;2:805–16.

13. Ellingsgaard H, Hauselmann I, Schuler B, Habib AM, Baggio LL, Meier DT, et al. Interleukin-6 enhances insulin secretion by increasing glucagon-like peptide-1 secretion from L cells and alpha cells. Nat Med. 2011;17:1481–9.

14. Hanahan D, Weinberg RA. Hallmarks of cancer: the next generation. Cell. 2011;144:646–74.

15. Faubert B, Solmonson A, DeBerardinis RJ. Metabolic reprogramming andcancer progression. Science. 2020;368.

16. Levine AJ, Jenkins NA, Copeland NG. The roles of initiating truncal mutations in human cancers: the order of mutations and tumor cell type matters. Cancer Cell. 2019;35:10–5.

17. Pavlova NN, Thompson CB. The emerging hallmarks of cancer metabolism. CellMetab. 2016;23:27–47.

18. Liberti MV, Locasale JW. The warburg effect: how does it benefit cancer cells? Trends Biochem Sci. 2016;41:211–8.

19. Fu Y, Liu S, Yin S, Niu W, Xiong W, Tan M, et al. The reverse Warburg effect is likely to be an Achilles' heel of cancer that can be exploited for cancer therapy. Oncotarget. 2017;8:57813–25.

20. Curtis M, Kenny HA, Ashcroft B, Mukherjee A, Johnson A, Zhang Y, et al. Fibroblasts mobilize tumor cell glycogen to promote proliferation and metastasis.Cell Metab. 2019;29:141-155.e9.

21. Nocquet L, Juin PP, Souazé F. Mitochondria at Center of Exchanges between Cancer Cells and Cancer-Associated Fibroblasts during Tumor Progression. Cancers (Basel). 2020;12.

22. Gentric G, Mechta-Grigoriou F. Tumor Cells and Cancer-Associated Fibroblasts: An Updated Metabolic Perspective. Cancers (Basel). 2021;13.

23. Nazemi M, Rainero E. Cross-Talk Between the Tumor Microenvironment, Extracellular Matrix, and Cell Metabolism in Cancer. Front Oncol. 2020;10:239.

24. Nieman KM, Kenny HA, Penicka CV, Ladanyi A, Buell-Gutbrod R, Zillhardt MR, et al. Adipocytes promote ovarian cancer metastasis and provide energy for rapidtumor growth. Nat Med. 2011;17:1498–503.

25. Karstoft K, Pedersen BK. Skeletal muscle as a gene regulatory endocrine organ. Curr Opin Clin Nutr Metab Care. 2016;19:270–5.

26. Elia I, Schmieder R, Christen S, Fendt S-M. Organ-Specific Cancer Metabolism and Its Potential for Therapy. Handb Exp Pharmacol. 2016;233:321–53.

27. American College of Sports Medicine, Riebe D, Ehrman JK 1962-, Liguori G 1965-, Magal M. ACSM's guidelines for exercise testing and prescription. Tenthedition. Philadelphia: Wolters Kluwer; 2018.

28. Priego T, Sánchez J, Picó C, Palou A. Sex-differential expression of metabolism-related genes in response to a high-fat diet. Obesity (Silver Spring). 2008;16:819–26.

29. Fainstein N, Tyk R, Touloumi O, Lagoudaki R, Goldberg Y, Agranyoni O, et al. Exercise intensity-dependent immunomodulatory effects on encephalomyelitis. Ann Clin Transl Neurol. 2019;6:1647–58.

30. Parikh R, Sorek E, Parikh S, Michael K, Bikovski L, Tshori S, et al. Skin

exposure to UVB light induces a skin-brain-gonad axis and sexual behavior. CellRep. 2021;36:109579.

31. The Uniprot Consortium . UniProt: a worldwide hub of protein knowledge The UniProt Consortium. Nucleic Acids Research. 2019;

32. Tyanova S, Temu T, Sinitcyn P, Carlson A, Hein MY, Geiger T, et al. The Perseus computational platform for comprehensive analysis of (prote)omics data.Nat Methods. 2016;13:731–40.

33. The Gene Ontology Consortium. The Gene Ontology resource: enriching a GOld mine. Nucleic Acids Res. 2021;49:D325–34.

34. Journe F, Id Boufker H, Van Kempen L, Galibert MD, Wiedig M, Salès F, et al. TYRP1 mRNA expression in melanoma metastases correlates with clinical outcome. Br J Cancer. 2011;105:1726–32.

35. Coker RH, Kjaer M. Glucoregulation during exercise : the role of the neuroendocrine system. Sports Med. 2005;35:575–83.

36. Chen LB. Mitochondrial membrane potential in living cells. Annu Rev Cell Biol. 1988;4:155–81.

37. Neufer PD, Bamman MM, Muoio DM, Bouchard C, Cooper DM, Goodpaster BH, et al. Understanding the Cellular and Molecular Mechanisms of Physical Activity-Induced Health Benefits. Cell Metab. 2015;22:4–11.

38. Cheeseman C, Long W. Structure of, and functional insight into the GLUT familyof membrane transporters. Cell Health Cytoskelet. 2015;167.

39. Wang T, Wang J, Hu X, Huang X-J, Chen G-X. Current understanding of glucose transporter 4 expression and functional mechanisms. World J Biol Chem. 2020;11:76–98.

40. Sylow L, Kleinert M, Richter EA, Jensen TE. Exercise-stimulated glucose uptake - regulation and implications for glycaemic control. Nat Rev Endocrinol.2017;13:133–48.

41. Clemmons DR. Involvement of insulin-like growth factor-I in the control ofglucose homeostasis. Curr Opin Pharmacol. 2006;6:620–5.

42. Netz Y, Goldsmith R, Shimony T, Ben-Moshe Y, Zeev A. Adherence to physical activity recommendations in older adults: an Israeli national survey. J Aging PhysAct. 2011;19:30–47.

43. Cohen G, Steinberg DM, Keinan-Boker L, Shaked O, Goshen A, Shimony T, et al. Leisure-Time Physical Activity and Cancer Risk Among Older Adults: A CohortStudy. Mayo Clin Proc Innov Qual Outcomes. 2020;4:115–25.

44. Moore E, Silverman BG, Fishler Y, Ben-Adiva E, Davidov O, Dichtiar R, et al. An assessment of the completeness and timeliness of the israel national cancer registry. Isr Med Assoc J. 2021;23:23–7.

45. National Cancer Registry, Ministry of Health [Internet]. [cited 2021 Dec 19].

46. Ballou LM, Lin RZ. Rapamycin and mTOR kinase inhibitors. J Chem Biol. 2008;1:27–36.

47. Dupuy F, Tabariès S, Andrzejewski S, Dong Z, Blagih J, Annis MG, et al. PDK1-Dependent Metabolic Reprogramming Dictates Metastatic Potential in Breast Cancer. Cell Metab. 2015;22:577–89.

48. Vander Heiden MG, DeBerardinis RJ. Understanding the Intersections between Metabolism and Cancer Biology. Cell. 2017;168:657–69.

49. Harel M, Ortenberg R, Varanasi SK, Mangalhara KC, Mardamshina M, Markovits E, et al. Proteomics of melanoma response to immunotherapy reveals mitochondrial dependence. Cell. 2019;179:236-250.e18.

50. Pitt JM, Vétizou M, Daillère R, Roberti MP, Yamazaki T, Routy B, et al. Resistance Mechanisms to Immune-Checkpoint Blockade in Cancer: Tumor-Intrinsic and -Extrinsic Factors. Immunity. 2016;44:1255–69.

51. Phan TG, Croucher PI. The dormant cancer cell life cycle. Nat Rev Cancer. 2020;20:398–411.

52. Vera-Ramirez L, Vodnala SK, Nini R, Hunter KW, Green JE. Autophagy promotes the survival of dormant breast cancer cells and metastatic tumourrecurrence. Nat Commun. 2018;9:1944.

53. Akins NS, Nielson TC, Le HV. Inhibition of glycolysis and glutaminolysis: an emerging drug discovery approach to combat cancer. Curr Top Med Chem. 2018;18:494–504.

54. Nguyen T, Kirsch BJ, Asaka R, Nabi K, Quinones A, Tan J, et al. Uncovering the Role of N-Acetyl-Aspartyl-Glutamate as a Glutamate Reservoir in Cancer. Cell Rep. 2019;27:491-501.e6.

55. Greger JG, Eastman SD, Zhang V, Bleam MR, Hughes AM, Smitheman KN, et al. Combinations of BRAF, MEK, and PI3K/mTOR inhibitors overcome acquired resistance to the BRAF inhibitor GSK2118436 dabrafenib, mediated by NRAS orMEK mutations. Mol Cancer Ther. 2012;11:909–20.

56. Kreuzaler P, Panina Y, Segal J, Yuneva M. Adapt and conquer: Metabolic flexibility in cancer growth, invasion and evasion. Mol Metab. 2020;33:83–101.

57. Zois CE, Harris AL. Glycogen metabolism has a key role in the cancer microenvironment and provides new targets for cancer therapy. J Mol Med.2016;94:137–54.

58. Takahashi Y, Sarkar J, Yamada J, Matsunaga Y, Nonaka Y, Banjo M, et al. Enhanced skeletal muscle glycogen repletion after endurance exercise is associated with higher plasma insulin and skeletal muscle hexokinase 2 protein levels in mice: comparison of level running and downhill running model. J PhysiolBiochem. 2021;77:469–80.

59. Hingst JR, Bruhn L, Hansen MB, Rosschou MF, Birk JB, Fentz J, et al. Exercise-induced molecular mechanisms promoting glycogen supercompensation in human skeletal muscle. Mol Metab. 2018;16:24–34.

60. Zitvogel L, Derosa L, Kroemer G. Modulation of cancer immunotherapy bydietary fibers and over-the-counter probiotics. Cell Metab. 2022;34:350–2.

61. Giles ED, Wellberg EA, Astling DP, Anderson SM, Thor AD, Jindal S, et al. Obesity and overfeeding affecting both tumor and systemic metabolism activatesthe progesterone receptor to contribute to postmenopausal breast cancer. Cancer Res. 2012;72:6490–501.

62. Taaffe DR, Marcus R. Dynamic muscle strength alterations to detraining and retraining in elderly men. Clinical Physiology. 1997;17:311–24.

63. Meyer K, Schwaibold M, Westbrook S, Beneke R, Hajric R, Görnandt L, et al. Effects of short-term exercise training and activity restriction on functional capacity in patients with severe chronic congestive heart failure. Am J Cardiol.1996;78:1017–22.

64. Gundersen K. Muscle memory and a new cellular model for muscle atrophy and hypertrophy. J Exp Biol. 2016;219:235–42.

65. Luo H, Galvão DA, Newton RU, Fairman CM, Taaffe DR. Sport medicine in the prevention and management of cancer. Integr Cancer Ther. 2019;18:1534735419894063.

Figure legends:

Fig. 1. Exercise causes a metabolic shift in tissues. A, Schematic representation of the exercise mouse model. **B,** Left: Heatmaps showing proteins differentially expressed in lungs, lymph, liver, and skeletal muscle of active mice versus control with red indicative of upregulation and green indicative of downregulation in the tissues of active mice. Right: Proteomaps of KEGG pathways enriched in differentially expressed proteins. **C and D,** Proteins differentially expressed in active mice enriched for (**C**) GO biological process and (**D**) GO cellular compartment identified using GENEONTOLOGY tool. Left: Venn diagram of overlap of the GO terms for proteins differentially expressed in the indicated organs for (**C**) biological processes and (**D**) cellular compartment. Right: Sum of fold enrichment of the GO terms for all the indicated tissues. **E**, Left: Glucose uptake in single cells originating from the indicated organs evaluated by analysis of fluorescence of 2-NBDG. Right: Mean green fluorescence intensity in single cells originating from the indicated organs of the control and active mice relative to intensity in control tissue. **F,** Glycolytic function of single cells from the indicated organs determined using ECAR measurements. Samples were normalized to their *Gapdh* mRNA level. Error bars represent ± SEM (n ≥ 4). **G,** FACS analysis of mitochondrial activity in primary organ cells (lungs, lymph nodes, liver and skeletal muscles) of control and active mice; TMRE expression is indicative of active mitochondria. Left panel: Representative image of the FACS data shows the $TMRE^-$ and $TMRE^+$ cell populations for control and active mice. Right panel: Quantification (% gated cells) from the FACS for control and active mice. Statistical comparison between $TMRE^-$ and $TMRE^+$ from each group (control and active) and $TMRE^+$ between control and active groups is presented in the graphs. (n > 3 animals in each group). * $p < 0.05$; ** $p < 0.01$; *** $p < 0.001$. **H,** qRT-PCR quantification of the mRNAs encoding the indicated glucose transporters in tissues from active and control mice. Data were normalized

to endogenous levels of *Gapdh* or *Hprt*. Error bars represent ± SEM (n = 3 independent experiments). * $p < 0.05$; ** $p < 0.01$; *** $p < 0.001$.

Fig. 2. High-intensity activities reduce metastatic cancer likelihood. **A,** Schematic representation of human exercise model. **B,** Venn diagrams showing an overlap of 16 pathways based on a GO enrichment analysis of differential proteins found in theplasma of the routinely active subjects (n = 3 males and n = 3 females) after 30-min run on treadmill. **C,** The top four GO-enriched pathways of the 16 overlapped GO terms. **D,** The relative contributions of carbohydrates (CHO) and fats to the total substrate utilization prior to exercise and during moderate and high-intensity during a graded exercise test performed on a motorized treadmill. **E**, Fold enrichments of Hazard Ratio (HR) from a prospective cohort study among 2,734 cancer free participants that was followed for 20 years, with indicated SEER stages of cancer were who were classified into inactive (ref), low-moderate intensity (<6 metabolic equivalent, MET) and high intensity exercise (>6 MET). 'w' indicates the analysis for propensity score weighted model. * $p < 0.05$. **F,** Relative exercise intensity of individuals with a cancer diagnosis during the 20 years of follow-up that were classified as SEER 0-4 compared to those with cancers classified as SEER 7.

Fig. 3. Exercise inhibits melanoma metastasis formation. **A,** Schematic of the subdermal melanoma mouse model. **B,** Left: Representative images of mice from the control and active groups. Right: Calculated tumor volumes. Error bars represent ± SEM (n = 16 mice per group). * $p < 0.05$, ** $p < 0.01$. **C,** Left: FACS analysis of single cells from the lymph nodes, lungs, and liver of control and active mice subdermally injected with *Ret*-mCherry-labeled melanoma cells. mCherry-negative stromal cells are in green

and mCherry-positive melanoma cells are in red. Right: Fold change in mCherry positive cells in active mice relative to controls based on the FACS analysis. Error bars represent ± SEM (n = 8 group). ** $p < 0.01$, *** $p < 0.001$. **D,** Experimental design for intra-carotid injection. Controls were sedentary. Active mice were exercised pre and post tumor cell injection or only pre injection. **E,** Left: Bioluminescence images of lungs taken from control and exercised mice. Right: Photon quantification of melanoma metastases plotted as fold change relative to control. Error bars represent ± SEM (n = 20 mice in control and active 'pre & post' groups). ** $p < 0.01$. **(f)** qRT-PCR quantification of melanoma markers *mCherry*, *Tyrp1*, and *Mlana* in the lungs of 'pre & post' group. Data were normalized to *Hprt* and are plotted relative to quantities in control mice. Error bars represent ± SEM (n ≥ 3 independent experiments). *** $p < 0.001$. **G,** Left: Bioluminescence images of melanoma in the lungs taken from control mice and mice exercised only before intra-carotid injection of tumor cells. Right: Photon quantification of melanoma metastases plotted as fold change relative to control. Error bars represent ± SEM (n = 8 mice in each group). *** $p < 0.001$. **H,** qRT-PCR quantification of melanoma markers *mCherry*, *Tyrp1*, and *Mlana* in the lungs of control mice and mice exercised only before intra-carotid injection of tumor cells. Data were normalized to *Hprt*. Error bars represent ± SEM (n ≥ 3 independent experiments). ***$p < 0.001$. **I,** Experimental design for the co-culture of the melanoma cells and primary cells for microscopy analysis. **J,** Left: Immunofluorescent images of melanoma cells that express mCherry seeded on adhered primary cells from the lymph nodes, lungs, and livers of control and active mice. Right: Percent melanoma cell numbers relative to total cell numbers quantified in brightfield images. Error bars represent ± SEM (n = 3

independent experiments). * $p < 0.05$. **K,** FACS analysis of GFP-labeled *Ret*-melanoma cells co-cultured with primary lung cells of control and active mice. GFP^+ (melanoma) and GFP^- (primary lung cells). Upper panel: Representational dot plots from FACS analysis. Lower panel: Calculation of GFP^+ positive cells based on the FACS analysis. Error bars represent ± SEM (n = 6 animals in each group). ** $p < 0.01$. **L,** FACS analysis of mCherry labeled *Ret*-melanoma with primary lung cells from active and control animals. Upper panel (vehicle treated): (Left) Representative image of % gatedof $mCherry^+$ cells with vehicle treated primary cells from active and control mice. (Right) Graph representing fold change of surviving melanoma cells co-cultured with either active or control primary cells. Lower Panel (rapamycin treated): (Left) Representative image of % gated of $mCherry^+$ cells with rapamycin (100 nM) treated primary cells from active and control mice. (Right) Graph representing fold change of surviving melanoma cells co-cultured with either active or control primary cells. Error bars represent ± SEM (n > 3 animals in each group). *** $p < 0.001$.

Fig. 4. Metabolic crosstalk between cancer cells and stroma. A, Left: Heatmap of the normalized expression of genes from TCGA data set (rows) classified as benign nevi, atypical nevi, vertical growth phase melanoma (VGP), and *in situ* melanoma compared to melanoma metastases of indicated tissues (Supplementary Table S3). Red indicates high expression; blue indicates low expression. Right: KEGG enrichment analysis of the genes up- and downregulated in metastatic melanoma. **B,** KEGG enrichment analysis if genes downregulated in primary melanomas of mice exercised pre and post melanoma cell injection compared to control mice (3). **C,** Upper: Experimental design for the co-culture of the melanoma cells and primary cells for

mitochondrial activity (stained by TMRE) by FACS (as indicated). Lower left: FACS analysis of mitochondrial activity in GFP-labeled *Ret*-melanoma cells co-cultured with primary lung cells of control and active mice; TMRE expression is indicative of active mitochondria. Lower right: Calculation of $TMRE^+$ cells in primary lung cells (upper) melanoma (lower) based on the FACS analysis. Error bars represent ± SEM (n = 6 animals in each group). * $p < 0.05$. **D,** Schematic representation of the glucose uptake assay**. E,** Upper and middle: FACS analysis of uptake of 2-NBDG by melanoma ($mCherry^+$) and stromal ($mCherry^-$) cells originating from the lungs and lymph nodes. Lower: Intensity of signal from 2-NBDG in stroma and melanoma from lungs and lymph of control and active mice. **F-G,** Left: Hematoxylin and eosin staining (20X magnification) and immunofluorescence analysis (40X magnification) of S100-Beta (green) and GLUT1, ALDOA, or COMPLEX I (red) in (**F**) lungs, (**G**) lymph nodes, and
(**H**) livers. DAPI-stained nuclei appear in blue. White-dashed lines indicate tumor (T) — stroma (S) boundaries. Right: Quantification of the red and green mean fluorescence intensities in the tumor and stroma normalized to DAPI mean fluorescence intensity using ImageJ. *t*-test statistical comparison represented as: * (black) indicates a *t*-test GLUT1, ALDOA or COMPLEX I (red) comparison of the control and active animals in stroma or tumor regions; + indicates a *t*-test GLUT1 (red), ALDOA (red), COMPLEX I (red) of S100-beta (green) comparison of the stroma and tumor regions of the control animals; indicates a *t*-test GLUT1 (red), ALDOA (red), COMPLEX I (red) or S100- Beta (green) comparison of the stroma and tumor regions of active animals. Error bars represent ± SEM (n>15 fields from each area (stroma or tumor for each target) in at

least three images). + or* or □ $p < 0.05$; ++ or ** or □□ $p < 0.001$; +++ or *** or □□□$p < 0.001$.

Fig. 1

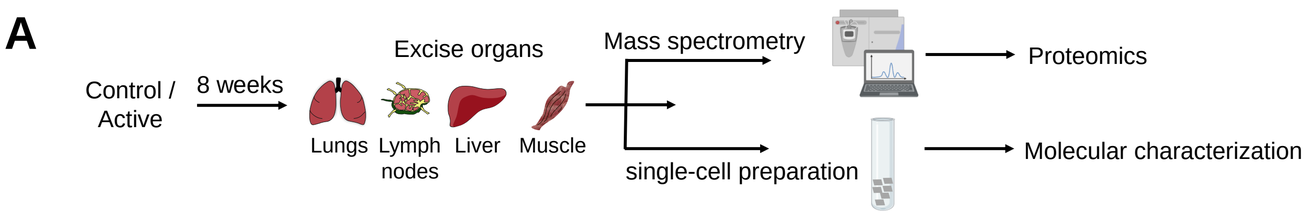

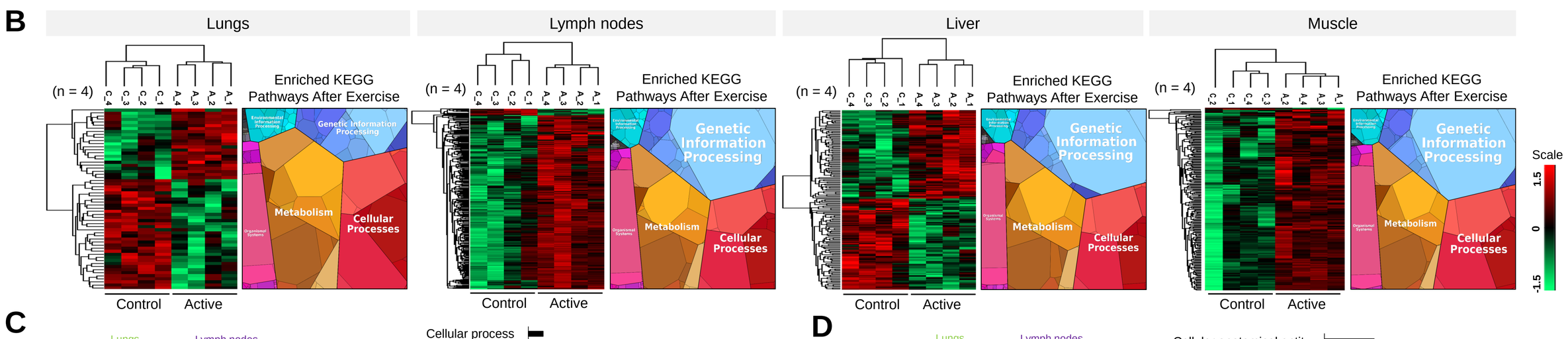

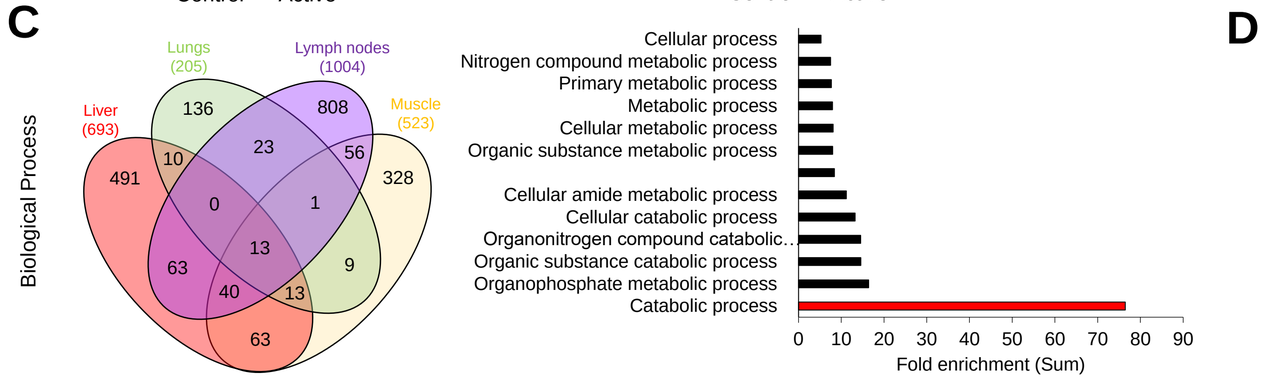

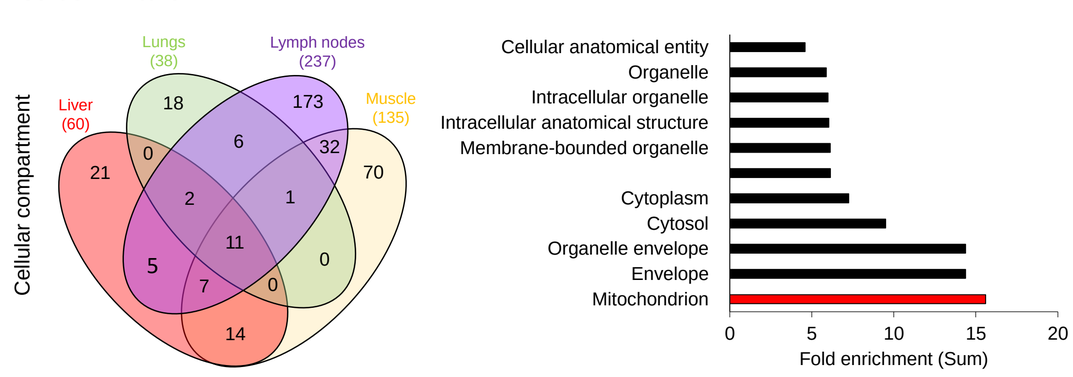

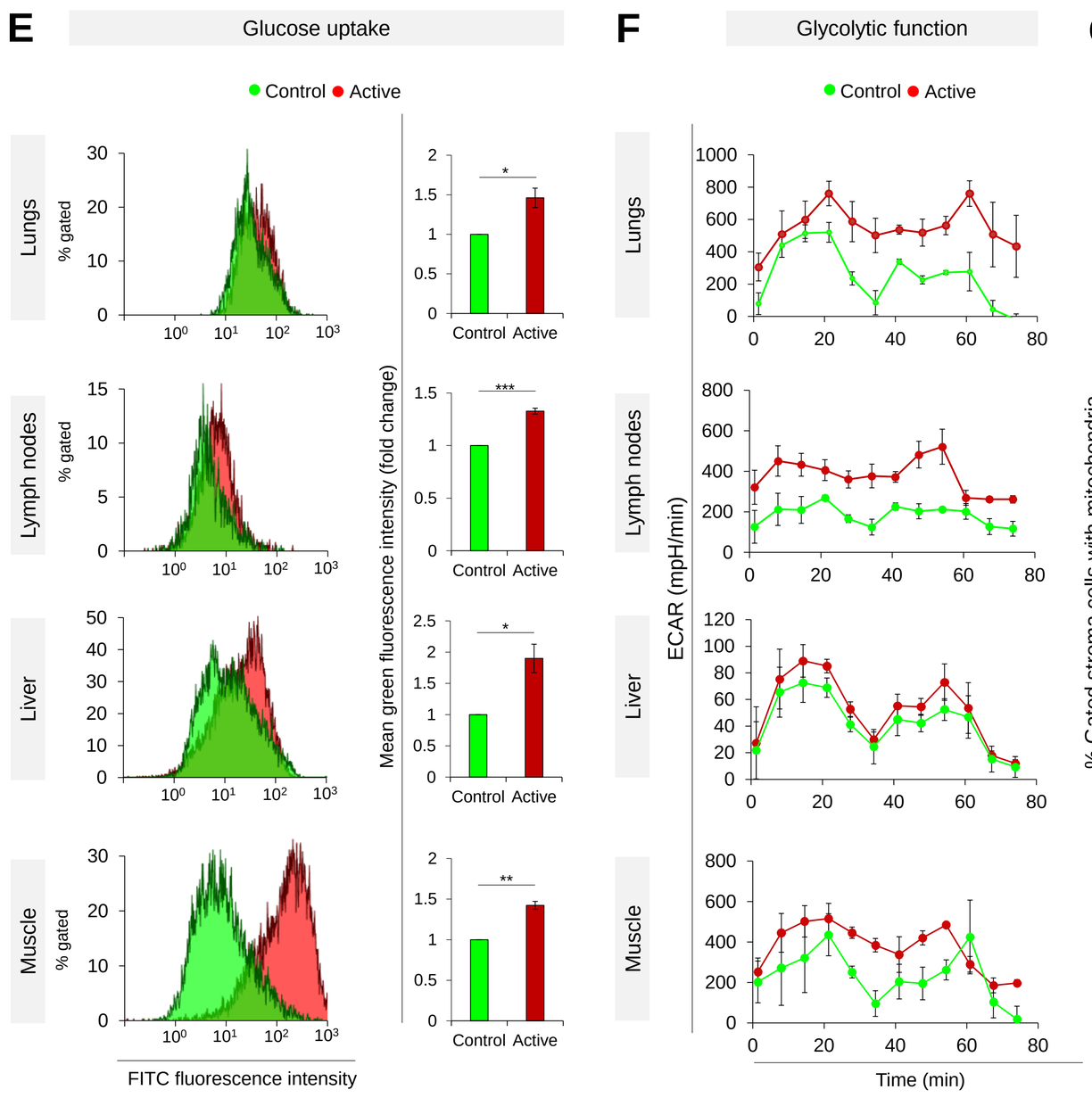

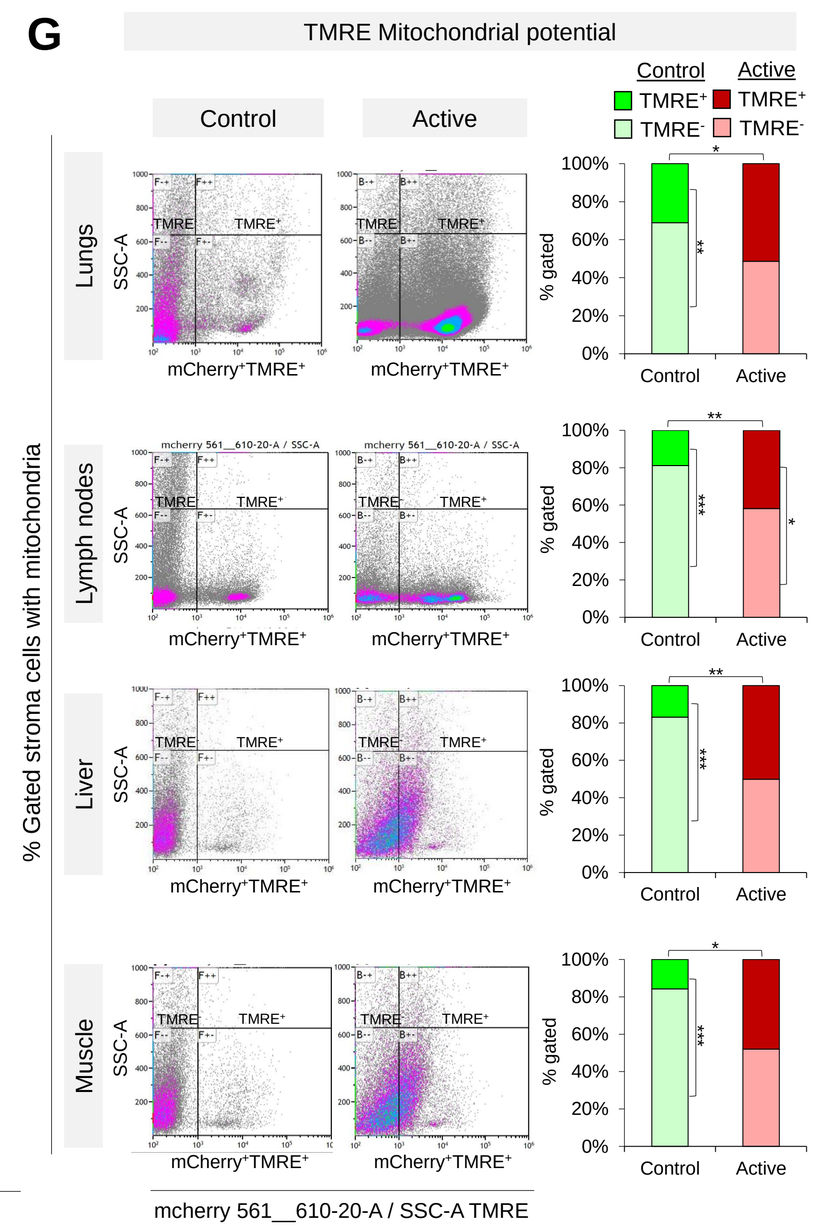

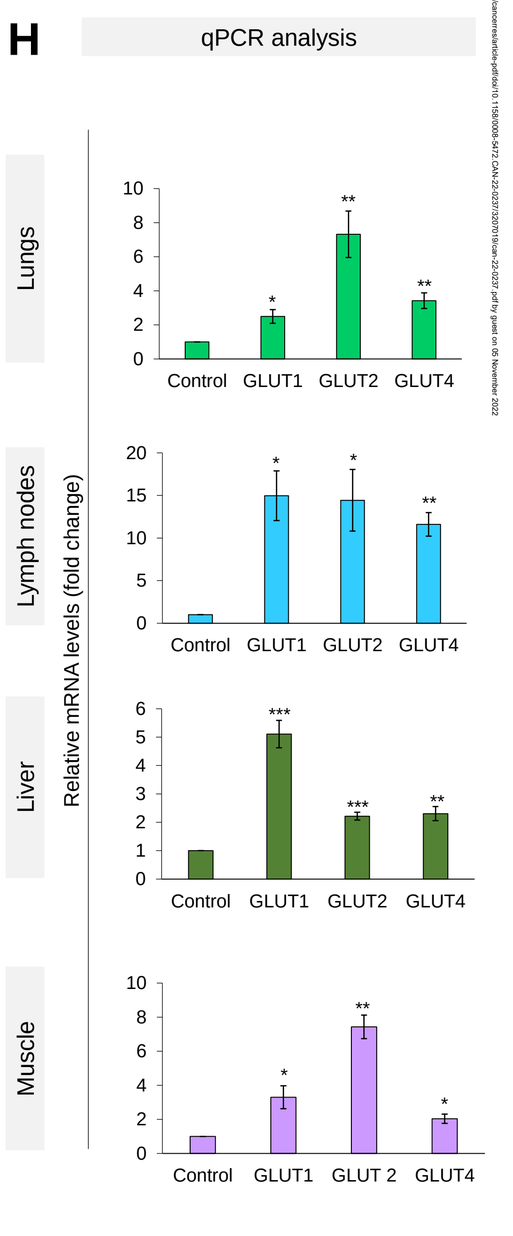

Fig. 2

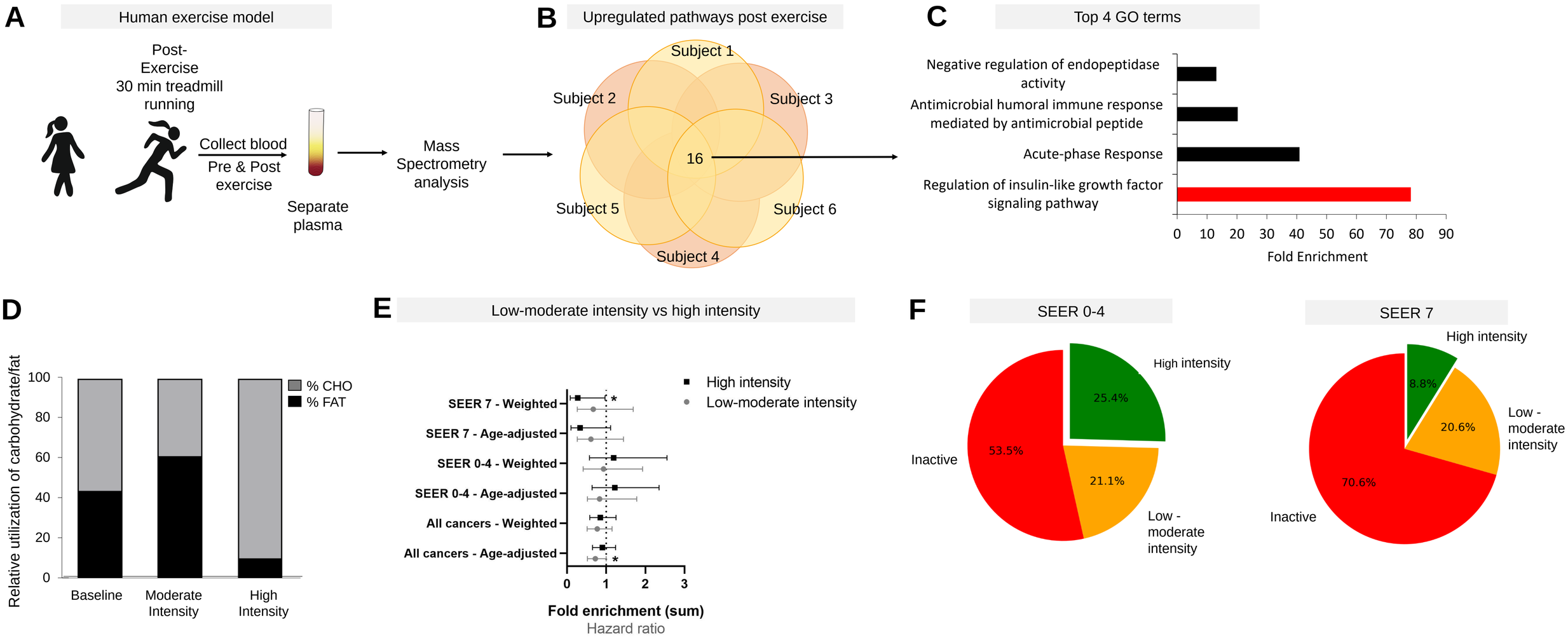

Fig. 3

Fig. 4